

# Single-particle spectral function of the $\Lambda$ hyperon in finite nuclei

Isaac Vidaña

*CFisUC, Department of Physics, University of Coimbra, PT-3004-516 Coimbra, Portugal*

*email: ividana@fis.uc.pt*

---

## Abstract

The spectral function of the  $\Lambda$  hyperon in finite nuclei is calculated from the corresponding  $\Lambda$  self-energy, which is constructed within a perturbative many-body approach using some of the realistic hyperon-nucleon interactions of the Jülich and Nijmegen groups. Binding energies, wave functions and disoccupation numbers of different single-particle states are obtained for various hypernuclei from  ${}^5_{\Lambda}\text{He}$  to  ${}^{209}_{\Lambda}\text{Pb}$ . The agreement between the calculated binding energies and experimental data is qualitatively good. The small spin-orbit splitting of the  $p$ -,  $d$ -,  $f$ - and  $g$ -wave states is confirmed. The discrete and the continuum contributions of the single- $\Lambda$  spectral function are computed. Their appearance is qualitatively similar to that of the nucleons. The  $\mathcal{Z}$ -factor, that measures the importance of correlations, is also calculated. Our results show that its value is relatively large, indicating that the  $\Lambda$  hyperon is less correlated than nucleons. This is in agreement with the results obtained by other authors for the correlations of the  $\Lambda$  in infinite nuclear matter. The disoccupation numbers are obtained by integrating the spectral function over the energy. Our results show that the contribution of the discrete part of the  $\Lambda$  self-energy is always much more smaller than the continuum one. This indicates that, in the production reactions of hypernuclei, the  $\Lambda$  hyperon is mostly formed in a quasi-free state.

*Keywords:* Hypernuclei; YN interaction;  $G$ -matrix; Self-energy; Spectral function; Correlations.

---

## 1. Introduction

The study of hypernuclei, bound systems composed of nucleons and one or more hyperons, provides a unique tool to extent our present knowledge of conventional nuclear physics to the  $SU(3)$ -flavour sector.

Hypernuclei were discovered in 1952 with the observation of a hyperfragment in a balloon-flown emulsion stack by Danysz and Pniewski [1]. These initial cosmic-ray observations of hypernuclei were followed later by pion and proton beam production reactions in emulsions and  ${}^4\text{He}$  bubble chambers. The weak decay of the  $\Lambda$  hyperon into a  $\pi^-$  plus a proton was used to identify different  $\Lambda$ -hypernuclei and to determine the binding energies, spins and lifetimes for hypernuclei up to  $A = 15$  [2, 3]. Average properties of heavier systems were estimated from spallation experiments, and two double- $\Lambda$  hypernuclei were reported from  $\Xi^-$  capture [4, 5, 6, 7, 8, 9, 10]. More systematic investigations of hypernuclei began with the advent of separated  $K^-$  beams,

which allowed to produce single  $\Lambda$ -hypernuclei through  $(K^-, \pi^-)$  *strangeness exchange reactions*, where a neutron hit by a  $K^-$  is changed into a  $\Lambda$  emitting a  $\pi^-$ . The analysis of these reactions, initially carried out at CERN and later at BNL, KEK and J-PARC, showed many of the hypernuclear characteristics such as, for instance, the small spin-orbit strength of the hyperon-nucleon (YN) interaction, or the fact that the  $\Lambda$  essentially retains its identity inside the nucleus. The use of  $\pi^+$  beams at BNL, KEK and GSI has permitted to perform  $(\pi^+, K^+)$  *associate production reactions*, where an  $s\bar{s}$  pair is created from the vacuum, and a  $K^+$  and a  $\Lambda$  are produced in the final state. The *electro-production* of hypernuclei at JLAB and MAMI-C by means of the reaction  $(e, e'K^+)$  provides a high precision tool for the study of hypernuclear spectroscopy [11] due to the excellent spatial and energy resolution of the electron beams. The HypHI collaboration at FAIR/GSI has recently proposed a completely new and alternative way to produce hypernuclei by using stable and unstable heavy ion beams [12]. A first experiment has been already performed using a  ${}^6\text{Li}$  beam on a  ${}^{12}\text{C}$  target at 2 A GeV, in which the  $\Lambda$  and the  ${}^3_{\Lambda}\text{H}$  and  ${}^4_{\Lambda}\text{H}$  hypernuclei have been observed [13].

Nowadays more than 40 single  $\Lambda$ -hypernuclei, and few double- $\Lambda$  [4, 5, 6, 7, 8, 9, 10, 14] and single- $\Xi$  [15, 16] ones have been identified. On the contrary, it has not been possible to prove without any ambiguity the existence of  $\Sigma$ -hypernuclei, which suggest that the  $\Sigma$ -nucleon interaction is most probably repulsive.

A simple theoretical description of  $\Lambda$ -hypernuclei consist of an ordinary nuclei with the  $\Lambda$  sitting in the single-particle states of an effective  $\Lambda$ -nucleus mean field potential. Several approaches, based on this simple description, have been used to study the properties of the  $\Lambda$  in finite nuclei. Woods-Saxon potentials, for instance, have been traditionally used to describe, in a shell model picture, the single-particle properties of the  $\Lambda$  from medium to heavy hypernuclei [17, 18, 19, 20]. Density dependent effects and non-localities have been included in non-relativistic Hartree–Fock calculations with Skyrme type YN interactions in order to improve the overall fit of the single-particle energies [21, 22, 23, 24, 25, 26, 27, 28, 29]. Hypernuclear structure calculations have been also performed on the framework of relativistic mean field theory [30, 31, 32, 33, 34, 35, 36, 37, 38, 39] and Dirac phenomenology [40, 41]. Several hypernuclear structure studies based on *ab-initio* approaches exist in the literature [42, 43, 44, 45, 46, 47, 48, 49, 50]. In these studies the single-particle properties of the  $\Lambda$  in the hypernucleus are derived from an effective YN  $G$ -matrix built from a realistic bare YN interaction which describes the scattering data in free space. Recently, a Quantum Monte Carlo calculation of single- and double- $\Lambda$  hypernuclei has also been done using two- and three-body forces between the  $\Lambda$  and the nucleons [51, 52].

In most of these approaches, the quality of the description of hypernuclei relies on the validity of the mean field picture. However, the correlations induced by the YN interaction can substantially change this picture and, therefore, should not be ignored. Whereas the correlations of nucleons in nuclear matter and finite nuclei have been extensively studied by many authors (see *e.g.*, Refs. [53, 54, 55, 56, 57, 58, 59, 60, 61, 62, 63, 64, 65, 66, 67, 68, 69, 70, 71] and references therein), the correlations of hyperons have not received so much attention up to date. To the best of our knowledge, the effect of the  $\Lambda$  correlations in nuclear matter, beyond the mean field description, have been only studied by Robertson and Dickhoff [72, 73]. These authors used the Green’s function formalism [74] to study for the first time the propagation of a  $\Lambda$  in nu-

clear matter. They calculated the spectral function and quasi-particle parameters of the  $\Lambda$  finding results qualitatively similar to those of the nucleons, and showed that the  $\Lambda$  is, in general, less correlated than the nucleons.

The knowledge of the single-particle spectral function of the  $\Lambda$  in finite nuclei is fundamental not only to determine up to which extent the mean field description of hypernuclei is valid, but also for a proper description of the cross section of the different production mechanism of hypernuclei. Information on the single- $\Lambda$  spectral function can be obtained from a combined analysis of data provided by *e.g.*,  $(e, e'K^+)$  reactions or other experiments with theoretical calculations. However, as far as we know, until now the single- $\Lambda$  spectral function in finite nuclei has never been calculated. The scope of this work is to determine it for a variety of hypernuclei. To such end, we use a perturbative many-body approach with realistic YN interaction to determine first the  $\Lambda$  self-energy in finite nuclei from which we can then obtain the single- $\Lambda$  spectral function and the  $\Lambda$  single-particle bound states for the different hypernuclei.

The manuscript is organized in the following way. In Sec. 2 we describe in detail the method employed to determine the  $\Lambda$  spectral function in finite nuclei. Results for the  $\Lambda$  self-energy, single-particle bound states, spectral function and disoccupation numbers in several hypernuclei from  ${}^5_{\Lambda}\text{He}$  to  ${}^{209}_{\Lambda}\text{Pb}$  are presented and discussed in Sec. 3. Finally, our main conclusions are summarized in Sec. 4.

## 2. Evaluation of the single- $\Lambda$ spectral function in finite nuclei

In this section we describe the calculation of the single- $\Lambda$  spectral function in a hypernucleus. The starting point of this calculation is a nuclear matter YN  $G$ -matrix evaluated in momentum space at fixed nuclear matter density, center-of-mass momentum and starting energy. This nuclear matter  $G$ -matrix is then used to construct a finite nucleus YN  $G$ -matrix from which we can obtain the self-energy of the  $\Lambda$  in the Brueckner–Hartree–Fock (BHF) approximation, and the corresponding spectral function, for different single-particle bound and scattering states of an effective hyperon-nucleus potential in several hypernuclei. The calculation is done using some of the realistic YN interactions of the Jülich [75, 76] and the Nijmegen [77, 78, 79] groups. The description of our calculation is presented in the following after some few general remarks on the evaluation of spectral functions.

### 2.1. General remarks

It is well known in quantum many-body theory that the propagation of a particle or a hole with incoming (outgoing) momentum  $\vec{k}$  ( $\vec{k}'$ ) and energy  $\omega$  that is added to a given  $N$ -particle system is described by the single-particle Green's function (or propagator)  $g(\vec{k}, \vec{k}', \omega)$ , which can be obtained by solving the Dyson equation [74]

$$g(\vec{k}, \vec{k}', \omega) = g^{(0)}(\vec{k}, \vec{k}', \omega) + \int d\vec{k}'' \int d\vec{k}''' g^{(0)}(\vec{k}, \vec{k}'', \omega) \Sigma(\vec{k}'', \vec{k}''', \omega) g(\vec{k}''', \vec{k}', \omega), \quad (1)$$

where  $g^{(0)}(\vec{k}, \vec{k}', \omega)$  is the free single-particle propagator and  $\Sigma(\vec{k}, \vec{k}', \omega)$  is the proper self-energy. Using a compact matrix notation, the solution of the Dyson equation can be formally written as

$$\mathbf{g} = (\mathbf{1} - \mathbf{g}^{(0)} \mathbf{\Sigma})^{-1} \mathbf{g}^{(0)}. \quad (2)$$

The spectral function  $S(\vec{k}, \omega)$  can be directly obtained from the Lehmann representation of the diagonal part of the propagator

$$g(\vec{k}, \vec{k}, \omega) = \int_{-\infty}^{\mu} d\omega' \frac{S_h(\vec{k}, \omega')}{\omega - \omega' - i\eta} + \int_{\mu}^{\infty} d\omega' \frac{S_p(\vec{k}, \omega')}{\omega - \omega' + i\eta}, \quad (3)$$

where  $\eta$  is an infinitesimal quantity,  $\mu$  is the chemical potential, and  $S_h(\vec{k}, \omega)$  and  $S_p(\vec{k}, \omega)$  are the hole and particle parts of the spectral function which give, respectively, the probability density of removing or adding a particle to the ground state of a  $N$ -particle system, and finding the resulting  $(N-1)$ - or  $(N+1)$ -system in an excited state of energy  $\mu - \omega$  (with  $\omega < \mu$ ) or  $\omega - \mu$  (with  $\omega > \mu$ ). Using the well known Plemelj integral relation  $\frac{1}{x \pm i\eta} = P\frac{1}{x} \mp i\pi\delta(x)$  in Eq. (3), one easily gets

$$S_h(\vec{k}, \omega) = \frac{1}{\pi} \text{Im} g(\vec{k}, \vec{k}, \omega), \quad \omega < \mu \quad (4)$$

and

$$S_p(\vec{k}, \omega) = -\frac{1}{\pi} \text{Im} g(\vec{k}, \vec{k}, \omega), \quad \omega > \mu. \quad (5)$$

Writing  $\Sigma(\vec{k}, \vec{k}', \omega) = \text{Re} \Sigma(\vec{k}, \vec{k}', \omega) + i \text{Im} \Sigma(\vec{k}, \vec{k}', \omega)$  in the solution of the Dyson equation, taking the imaginary part of the propagator, and replacing it in Eqs. (4) and (5) one can express  $S_h(\vec{k}, \omega)$  and  $S_p(\vec{k}, \omega)$  in terms of the diagonal part of the self-energy simply as

$$S_h(\vec{k}, \omega) = \frac{1}{\pi} \frac{\text{Im} \Sigma(\vec{k}, \vec{k}, \omega)}{\left( \omega - \frac{\hbar^2 k^2}{2m} - \text{Re} \Sigma(\vec{k}, \vec{k}, \omega) \right)^2 + \left( \text{Im} \Sigma(\vec{k}, \vec{k}, \omega) \right)^2}, \quad \omega < \mu \quad (6)$$

and

$$S_p(\vec{k}, \omega) = -\frac{1}{\pi} \frac{\text{Im} \Sigma(\vec{k}, \vec{k}, \omega)}{\left( \omega - \frac{\hbar^2 k^2}{2m} - \text{Re} \Sigma(\vec{k}, \vec{k}, \omega) \right)^2 + \left( \text{Im} \Sigma(\vec{k}, \vec{k}, \omega) \right)^2}, \quad \omega > \mu, \quad (7)$$

where we have used the explicit expression of the diagonal part of the free single-particle propagator

$$g^{(0)}(\vec{k}, \vec{k}, \omega) = \frac{\theta(k_F - |\vec{k}|)}{\omega - \frac{\hbar^2 k^2}{2m} - i\eta} + \frac{\theta(|\vec{k}| - k_F)}{\omega - \frac{\hbar^2 k^2}{2m} + i\eta}. \quad (8)$$

Note that in Eqs. (6), (7) and (8) the energy  $\omega$  of the added particle or hole is measured with respect to its rest mass.

Being  $S_h(\vec{k}, \omega)$  and  $S_p(\vec{k}, \omega)$  probability densities, they are *non-negative* by definition and fulfil, for any value of the momentum  $\vec{k}$ , the following sum rule

$$\int_{-\infty}^{\mu} d\omega S_h(\vec{k}, \omega) + \int_{\mu}^{\infty} d\omega S_p(\vec{k}, \omega) = 1, \quad (9)$$

where the first integral determines the momentum distribution,  $n(\vec{k})$ , and the second one, the so-called depletion or disoccupation,  $d(\vec{k})$ .

After these general considerations let us now focus on the case of the  $\Lambda$  hyperon. As it is said in the introduction, its spectral function is crucial for the calculation of the production cross section of single- $\Lambda$  hypernuclei. It is clear that in any of the production mechanisms of single- $\Lambda$  hypernuclei the  $\Lambda$  can only be added to the system and, therefore, the hole part of its spectral function is zero. The Lehmann representation of the single- $\Lambda$  propagator is then simply

$$g_\Lambda(\vec{k}, \vec{k}, \omega) = \int_{\mu_\Lambda}^{\infty} d\omega' \frac{S_{p\Lambda}(\vec{k}, \omega')}{\omega - \omega' + i\eta}, \quad (10)$$

where the  $\Lambda$  chemical potential is given by

$$\mu_\Lambda = E(^{A+1}_\Lambda Z) - E(^A Z), \quad (11)$$

being  $E(^{A+1}_\Lambda Z)$  and  $E(^A Z)$  the ground state energies of the hypernucleus  $^{A+1}_\Lambda Z$  and the nucleus  $^A Z$ , respectively.

Similarly, the sum rule expressed by Eq. (9) is simplified, reading in this case

$$\int_{\mu_\Lambda}^{\infty} d\omega S_{p\Lambda}(\vec{k}, \omega) = 1, \quad (12)$$

which reflects the fact that is always possible to add a  $\Lambda$  to the system because the disoccupation of any  $\Lambda$ -state of momentum  $\vec{k}$  is 1.

## 2.2. $\Lambda$ self-energy in finite nuclei

Our calculation of the  $\Lambda$  self-energy is based on a method that was originally developed to study the properties of the nucleon [80] and the  $\Delta$  isobar [81] in finite nuclei, and was later extended to study those of the  $\Lambda$  and  $\Sigma$  hyperons [48, 49, 50]. In the following we present a general description of this method and refer the interested reader to these works, in particular to Refs. [48, 49, 50], for specific details of the calculation.

The evaluation of the  $\Lambda$  self-energy in finite nucleus stars with the construction of all the YN  $G$ -matrices which describe the in-medium interaction between a hyperon ( $Y = \Lambda, \Sigma$ ) and a nucleon in infinite nuclear matter. The  $G$ -matrices are obtained by solving the coupled-channel Bethe–Goldstone equation which schematically reads

$$\begin{aligned} \langle Y'N' | G | YN \rangle &= \langle Y'N' | V | YN \rangle + \sum_{Y''N'' = \Lambda N, \Sigma N} \langle Y'N' | V | Y''N'' \rangle \\ &\times \frac{Q_{Y''N''}}{\Omega - \varepsilon_{Y''} - \varepsilon_{N''} + i\eta} \langle Y''N'' | G | YN \rangle, \end{aligned} \quad (13)$$

where  $V$  is the bare YN interaction,  $Q_{Y''N''}$  is the Pauli operator, that prevents the nucleon in the intermediate state  $Y''N''$  to be scattered below its Fermi momentum  $k_{F_N}$ , and  $\Omega$  is the so-called starting energy which is the sum of the non-relativistic single-particle energies of the interacting hyperon and nucleon. We note here that the Bethe–Goldstone equation has been solved in momentum space in the partial wave basis  $|YN\rangle \equiv |K\mathcal{L}qLSJJTM_T\rangle$  where  $K(q)$  and  $\mathcal{L}(L)$  are respectively the center-of-mass (relative) momentum and orbital angular momentum,  $S$  is

the total spin,  $T$  and  $M_T$  are the total isospin and its third component, and  $\vec{J} = \vec{L} + \vec{S}$ . We note also that when solving it, the so-called discontinuous prescription has been adopted, *i.e.*, the single-particle energy of the hyperon ( $\varepsilon_{Y''}$ ) and the nucleon ( $\varepsilon_{N''}$ ) in the intermediate state  $Y''N''$  is taken simply as the sum of the non-relativistic kinetic energy plus the mass of the corresponding baryon. Finally, we should mention that our calculation has been done at nuclear matter density  $\rho = 0.17 \text{ fm}^{-3}$ , zero center-of-mass momentum and  $\Omega = m_N + m_\Lambda - 80 \text{ MeV}$ , where  $-80 \text{ MeV}$  is an averaged value for the sum of the single-particle mean fields of the nucleon ( $U_N(k = k_{FN}) \approx -50 \text{ MeV}$ ) and the  $\Lambda$  ( $U_\Lambda(k = 0) \approx -30 \text{ MeV}$ ) at this density. The dependence of our results on the values of the nuclear matter density  $\rho$  and the starting energy  $\Omega$  is weak as it is shown *e.g.*, in Refs. [49, 50].

The finite nucleus YN  $G$ -matrix,  $G_{FN}$ , can be obtained, in principle, by solving the Bethe–Goldstone equation directly in the finite nucleus (see *e.g.*, Refs. [82, 83]) which is formally identical to Eq. (13), being the only differences the Pauli operator and the energy denominator which in this case are the ones corresponding to the finite nucleus case. Alternatively, one can find  $G_{FN}$  by relating it to the nuclear matter  $G$ -matrix already obtained. Eliminating the bare interaction  $V$  in both finite nucleus and nuclear matter Bethe–Goldstone equations,  $G_{FN}$  can be written in terms of  $G$  through the following integral equation, written in a simplified form as

$$\begin{aligned} G_{FN} &= G + G \left[ \frac{Q_{FN}}{E_{FN}} - \frac{Q}{E} \right] G_{FN} \\ &= G + G \left[ \frac{Q_{FN}}{E_{FN}} - \frac{Q}{E} \right] G + G \left[ \frac{Q_{FN}}{E_{FN}} - \frac{Q}{E} \right] G \left[ \frac{Q_{FN}}{E_{FN}} - \frac{Q}{E} \right] G + \dots, \end{aligned} \quad (14)$$

where the difference  $Q_{FN}/E_{FN} - Q/E$  (being  $Q_{FN}$ ,  $E_{FN}$ ,  $Q$  and  $E$  the corresponding finite nucleus and nuclear matter Pauli operators and energy denominators) accounts for the relevant intermediate particle-particle states. This difference has been shown to be quite small [48, 49, 50, 80, 81] and, therefore, in all practical calculations  $G_{FN}$  can be well approximated by truncating the expansion (14) up second order in the nuclear matter  $G$ -matrix. Therefore, we have

$$G_{FN} \simeq G + G \left[ \frac{Q_{FN}}{E_{FN}} - \frac{Q}{E} \right] G. \quad (15)$$

Using now  $G_{FN}$  as an effective YN interaction, we can calculate the finite nucleus  $\Lambda$  self-energy in the BHF approximation (see diagram (a) of Fig. 1). According to Eq. (15) this approximation can be split into the sum of two contributions: the one of diagram (b), which represents the first-order term on the right-hand side of Eq. (15), and that of diagram (c), which stands for the so-called *two-particle-one-hole* ( $2p1h$ ) correction. In the following we show the explicit expressions of both contributions without going into many details of their derivation which can be found in Refs. [48, 49, 50].

Diagram (b) of Fig. 1 gives the following real and energy-independent contribution to the  $\Lambda$  self-energy

$$\begin{aligned} \mathcal{V}_1(k_\Lambda, k'_\Lambda, l_\Lambda, j_\Lambda) &= \frac{1}{2j_\Lambda + 1} \sum_{\mathcal{J}} \sum_{n_h l_h j_h t_{z_h}} (2\mathcal{J} + 1) \\ &\quad \times \langle (k'_\Lambda l_\Lambda j_\Lambda) (n_h l_h j_h t_{z_h}) \mathcal{J} | G | (k_\Lambda l_\Lambda j_\Lambda) (n_h l_h j_h t_{z_h}) \mathcal{J} \rangle, \end{aligned} \quad (16)$$

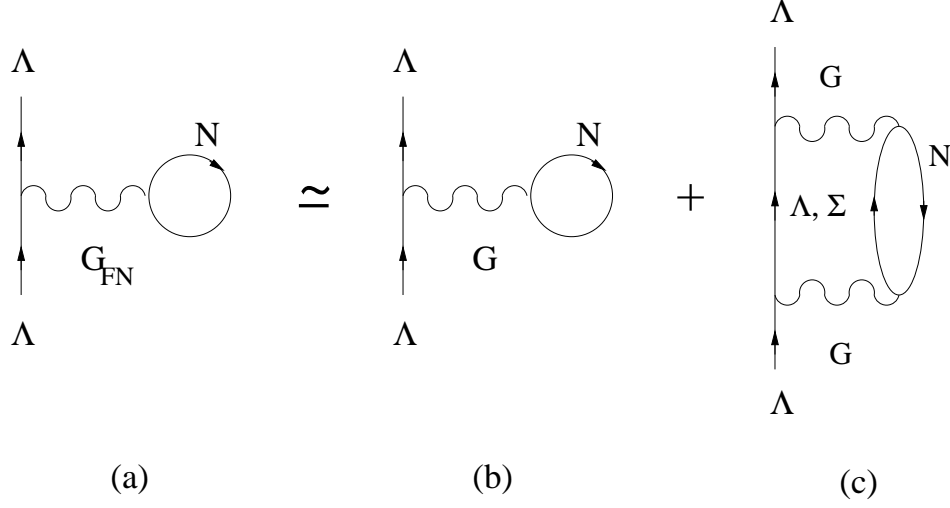


Figure 1: Brueckner-Hartree-Fock approximation of the finite nucleus  $\Lambda$  self-energy (diagram (a)), split into the sum of a first-order contribution (diagram (b)) and a second-order 2p1h correction (diagram (c)).

where the incoming (outgoing)  $\Lambda$  and the nucleon hole are respectively taken as plane wave and harmonic oscillator states with quantum numbers  $k_\Lambda(k'_\Lambda)l_\Lambda j_\Lambda$  and  $n_h l_h j_h t_{z_h}$ . The total angular momentum of the  $\Lambda$  nucleon hole pair is  $\vec{\mathcal{J}} = \vec{j}_\Lambda + \vec{j}_h$  in the laboratory frame. Note that in the above expression and in the following ones neither the z-component of the  $\Lambda$  isospin  $t_{z_\Lambda} = 0$  nor its total spin and that of the nucleons is shown explicitly.

The contribution of diagram (c) is the sum of two terms. The first of them is the term  $G(Q_{FN}/E_{FN})G$  in Eq. (15) which gives rise to an imaginary part in the  $\Lambda$  self-energy which depends explicitly on the energy of the hyperon and reads

$$\begin{aligned}
\mathcal{W}_{2p1h}(k_\Lambda, k'_\Lambda, l_\Lambda, j_\Lambda, \omega) = & -\frac{\pi}{2j_\Lambda + 1} \sum_{n_h l_h j_h t_{z_h}} \sum_{\mathcal{L} L S J \mathcal{J} Y' = \Lambda \Sigma} \sum_{Y' = \Lambda \Sigma} \int dq q^2 \int dK K^2 (2\mathcal{J} + 1) \\
& \times \langle (k'_\Lambda l_\Lambda j_\Lambda) (n_h l_h j_h t_{z_h}) \mathcal{J} | G | K \mathcal{L} q L S J \mathcal{J} T M_T \rangle \\
& \times \langle K \mathcal{L} q L S J \mathcal{J} T M_T | G | (k_\Lambda l_\Lambda j_\Lambda) (n_h l_h j_h t_{z_h}) \mathcal{J} \rangle \\
& \times \delta \left( \omega + \varepsilon_h - \frac{\hbar^2 K^2}{2(m_N + m_{Y'})} - \frac{\hbar^2 q^2 (m_N + m_{Y'})}{2m_N m_{Y'}} - m_{Y'} + m_\Lambda \right), \tag{17}
\end{aligned}$$

where  $\omega$  is the energy of the  $\Lambda$  measured with respect to its rest mass. The quantum numbers  $K, \mathcal{L}, q, L, S, J, \mathcal{J}, T$  and  $M_T$  have been defined before, and the energies of the nucleon hole states  $\varepsilon_h$  have been taken equal to the experimental single-particle ones of the nuclei studied. One can see from the delta function that  $\mathcal{W}_{2p1h}$  is different from zero only for positive values of  $\omega$ . The contribution of this term to the real part of the  $\Lambda$  self-energy can be obtained through the

following dispersion relation

$$\mathcal{V}_{2p1h}^{(1)}(k_\Lambda, k'_\Lambda, l_\Lambda, j_\Lambda, \omega) = \frac{1}{\pi} \mathcal{P} \int_{-\infty}^{\infty} d\omega' \frac{\mathcal{W}_{2p1h}(k_\Lambda, k'_\Lambda, l_\Lambda, j_\Lambda, \omega')}{\omega' - \omega}, \quad (18)$$

where  $\mathcal{P}$  stands for a principal value integral.

The second contribution of diagram (c) is that of the term  $G(Q/E)G$  in Eq. (15). This term gives also a real and energy-independent contribution to the  $\Lambda$  self-energy, and avoids double counting over intermediate  $Y'N$  states that are already contained in the nuclear matter  $G$ -matrix of the contribution of diagram (b). It reads

$$\begin{aligned} \mathcal{V}_{2p1h}^{(2)}(k_\Lambda, k'_\Lambda, l_\Lambda, j_\Lambda) &= \frac{1}{2j_\Lambda + 1} \sum_{n_h l_h j_h t_{z_h}} \sum_{\mathcal{L} \mathcal{L} S J J} \sum_{Y' = \Lambda \Sigma} \int dq q^2 \int dK K^2 (2\mathcal{J} + 1) \\ &\times \langle (k'_\Lambda l_\Lambda j_\Lambda)(n_h l_h j_h t_{z_h}) \mathcal{J} | G | K \mathcal{L} q \mathcal{L} S J \mathcal{J} T M_T \rangle \\ &\times \langle K \mathcal{L} q \mathcal{L} S J \mathcal{J} T M_T | G | (k_\Lambda l_\Lambda j_\Lambda)(n_h l_h j_h t_{z_h}) \mathcal{J} \rangle \\ &\times Q_{Y'N} \left( \Omega - \frac{\hbar^2 K^2}{2(m_N + m_{Y'})} - \frac{\hbar^2 q^2 (m_N + m_{Y'})}{2m_N m_{Y'}} - m_{Y'} + m_\Lambda \right)^{-1}, \end{aligned} \quad (19)$$

where  $Q_{Y'N}$  is the Pauli operator and  $\Omega$  is the starting energy introduced before in Eq. (13).

Further details on the evaluation of the  $\Lambda$  self-energy, such as the transformation from the basis  $|(k_\Lambda l_\Lambda j_\Lambda)(n_h l_h j_h t_{z_h}) \mathcal{J}\rangle$  to the partial wave one  $|K \mathcal{L} q \mathcal{L} S J \mathcal{J} T M_T\rangle$  used to solve Eq. (13), or the orthogonalization procedure of the occupied nucleon states with the distorted plane wave associated with the nucleon in the intermediate state of diagram (c), can be found in Refs. [48, 49, 50, 80, 81].

Summarizing, the BHF approximation of the self-energy of a  $\Lambda$  with incoming (outgoing) momentum  $k_\Lambda$  ( $k'_\Lambda$ ), orbital angular momentum  $l_\Lambda$ , and total angular momentum  $j_\Lambda$  is given by

$$\Sigma_{BHF}(k_\Lambda, k'_\Lambda, l_\Lambda, j_\Lambda, \omega) = \mathcal{V}(k_\Lambda, k'_\Lambda, l_\Lambda, j_\Lambda, \omega) + i\mathcal{W}(k_\Lambda, k'_\Lambda, l_\Lambda, j_\Lambda, \omega), \quad (20)$$

where the real and imaginary parts are

$$\mathcal{V}(k_\Lambda, k'_\Lambda, l_\Lambda, j_\Lambda, \omega) = \mathcal{V}_1(k_\Lambda, k'_\Lambda, l_\Lambda, j_\Lambda) + \mathcal{V}_{2p1h}^{(1)}(k_\Lambda, k'_\Lambda, l_\Lambda, j_\Lambda, \omega) - \mathcal{V}_{2p1h}^{(2)}(k_\Lambda, k'_\Lambda, l_\Lambda, j_\Lambda) \quad (21)$$

and

$$\mathcal{W}(k_\Lambda, k'_\Lambda, l_\Lambda, j_\Lambda, \omega) = \mathcal{W}_{2p1h}(k_\Lambda, k'_\Lambda, l_\Lambda, j_\Lambda, \omega). \quad (22)$$

### 2.3. $\Lambda$ spectral function

In any production mechanism of single- $\Lambda$  hypernuclei, a  $\Lambda$  with quantum numbers  $k_\Lambda l_\Lambda j_\Lambda$  can be formed either in a scattering or in a bound state. Therefore, its spectral function is the sum of a continuum and a discrete contribution

$$S_{p_\Lambda}(k_\Lambda, l_\Lambda, j_\Lambda, \omega) = S_{p_\Lambda}^c(k_\Lambda, l_\Lambda, j_\Lambda, \omega) + S_{p_\Lambda}^d(k_\Lambda, l_\Lambda, j_\Lambda, \omega), \quad (23)$$

which give, respectively, the probability density of adding the  $\Lambda$  in the scattering or the bound state of the corresponding hyperon-nucleus potential.

The continuum contribution is different from zero only for  $\omega \geq 0$  (see Eq. (17)) and it can be obtained by using the self-energy of Eq. (20) in Eq. (7). It simply reads

$$S_{p\Lambda}^c(k_\Lambda, l_\Lambda, j_\Lambda, \omega) = -\frac{1}{\pi} \frac{\mathcal{W}(k_\Lambda, k_\Lambda, l_\Lambda, j_\Lambda, \omega)}{\left(\omega - \frac{\hbar^2 k_\Lambda^2}{2m_\Lambda} - \mathcal{V}(k_\Lambda, k_\Lambda, l_\Lambda, j_\Lambda, \omega)\right)^2 + \left(\mathcal{W}(k_\Lambda, k_\Lambda, l_\Lambda, j_\Lambda, \omega)\right)^2}, \quad \omega \geq 0. \quad (24)$$

The discrete contribution is a weighted delta function located at the energy corresponding to the  $\Lambda$  bound state. To calculate it, we need first to determine this state. This can be done by using the real part of the  $\Lambda$  self-energy as an effective single-particle hyperon-nucleus potential in the Schrödinger equation. Following the procedure outlined in Refs. [48, 49, 50, 80, 81], we solve it by diagonalizing the corresponding single-particle Hamiltonian in a complete and orthonormal set of regular basis functions within a spherical box of radius  $R_{box}$  given in coordinate representation by

$$\Phi_{nl_\Lambda j_\Lambda m_{j_\Lambda}}(\vec{r}) = \langle \vec{r} | k_n l_\Lambda j_\Lambda m_{j_\Lambda} \rangle = N_{nl_\Lambda} j_\Lambda(k_n r) \psi_{l_\Lambda j_\Lambda m_{j_\Lambda}}(\theta, \phi), \quad (25)$$

where  $N_{nl_\Lambda}$  is a normalization constant

$$N_{nl_\Lambda} = \begin{cases} \frac{\sqrt{2}}{\sqrt{R_{box}^3} j_{l_\Lambda-1}(k_n R_{box})} & \text{for } l_\Lambda > 0 \\ \frac{n\sqrt{2}}{\sqrt{R_{box}^3}} & \text{for } l_\Lambda = 0, \end{cases} \quad (26)$$

$\psi_{l_\Lambda j_\Lambda m_{j_\Lambda}}(\theta, \phi)$  represents the spherical harmonics including the spin degree of freedom, and  $j_{l_\Lambda}(k_n r)$  denote the spherical Bessel functions for the discrete momenta  $k_n$  which can be obtained from the condition

$$j_{l_\Lambda}(k_n R_{box}) = 0. \quad (27)$$

To guarantee the independence of the results on  $R_{box}$ , its value should be larger than the radius of the nucleus considered. Typically  $R_{box}$  is chosen around 20 fm or larger. The resulting eigenvalue problem reads

$$\sum_{i=1}^{N_{max}} \left[ \frac{\hbar^2 k_i^2}{2m_\Lambda} + V(k_n, k_i, l_\Lambda, j_\Lambda, \omega = \varepsilon_{l_\Lambda j_\Lambda}) \right] \Psi_{il_\Lambda j_\Lambda m_{j_\Lambda}} = \varepsilon_{l_\Lambda j_\Lambda} \Psi_{nl_\Lambda j_\Lambda m_{j_\Lambda}}, \quad (28)$$

where the maximum number of basis states in the box,  $N_{max}$ , is typically restricted to 20 or 30, and  $\Psi_{nl_\Lambda j_\Lambda m_{j_\Lambda}} \equiv \langle k_n l_\Lambda j_\Lambda m_{j_\Lambda} | \Psi \rangle$  denotes the projection of the state  $|\Psi\rangle$  on the basis  $|k_n l_\Lambda j_\Lambda m_\Lambda\rangle$ . Note that a self-consistent procedure is required for each eigenvalue, *i.e.*, the  $\Lambda$  self-energy should be evaluated at each step of the iterative process at the energy of the resulting eigenvalue until convergence is achieved.

Once the solution of the Schrödinger equation is found we can finally obtain the contribution of this bound state to the  $\Lambda$  spectral function for the set of discrete momenta  $k_\Lambda = k_n$  simply as

$$S_{p\Lambda}^d(k_n, l_\Lambda, j_\Lambda, \omega) = Z_{l_\Lambda j_\Lambda} | \langle k_n l_\Lambda j_\Lambda m_{j_\Lambda} | \Psi \rangle |^2 \delta(\omega - \varepsilon_{l_\Lambda j_\Lambda}), \quad (29)$$

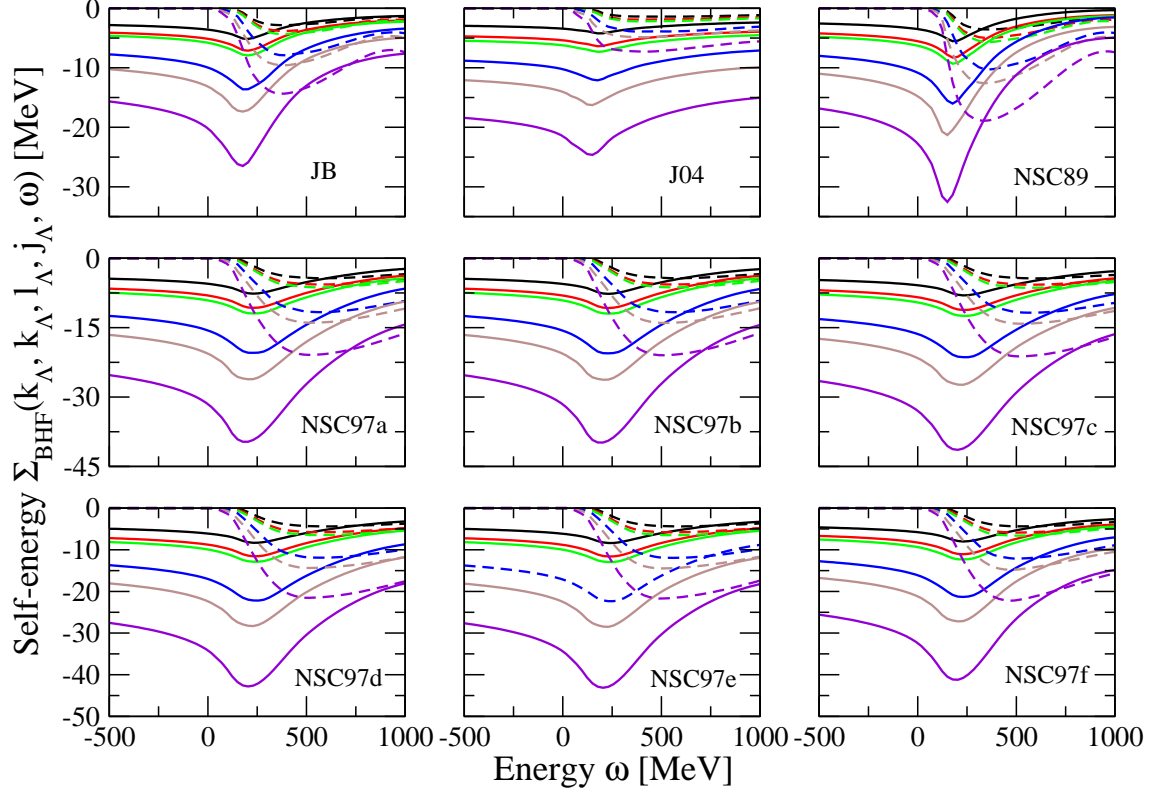


Figure 2: (color online) Energy dependence of the real  $\mathcal{V}$  (solid lines) and imaginary  $\mathcal{W}$  (dashed lines) part of the self-energy of a  $\Lambda$  with momentum of 300 MeV/c,  $l_\Lambda = 0$  and  $j_\Lambda = 1/2$  for  ${}^5_\Lambda\text{He}$  (black),  ${}^{13}_\Lambda\text{C}$  (red),  ${}^{17}_\Lambda\text{O}$  (green),  ${}^{41}_\Lambda\text{Ca}$  (blue),  ${}^{91}_\Lambda\text{Zr}$  (brown) and  ${}^{209}_\Lambda\text{Pb}$  (violet) obtained with the different YN interactions. The energy is measured with respect to the  $\Lambda$  rest mass.

where

$$Z_{l_\Lambda j_\Lambda} = \left( 1 - \frac{\partial \langle \Psi | \Sigma_{BHF}(\omega) | \Psi \rangle}{\partial \omega} \Big|_{\omega = \varepsilon_{l_\Lambda j_\Lambda}} \right)^{-1} \quad (30)$$

is the so-called spectroscopic factor [56] with the expectation value of the self-energy is given by

$$\langle \Psi | \Sigma_{BHF}(\omega) | \Psi \rangle = \sum_{i,n=1}^{N_{max}} \Psi_{i l_\Lambda j_\Lambda m_{j_\Lambda}}^* \Sigma_{BHF}(k_i, k_n, l_\Lambda, j_\Lambda, \omega) \Psi_{n l_\Lambda j_\Lambda m_{j_\Lambda}}. \quad (31)$$

### 3. Results

In this section we present our results for the self-energy, single-particle bound states and the spectral function of a  $\Lambda$  in  ${}^5_\Lambda\text{He}$ ,  ${}^{13}_\Lambda\text{C}$ ,  ${}^{17}_\Lambda\text{O}$ ,  ${}^{41}_\Lambda\text{Ca}$ ,  ${}^{91}_\Lambda\text{Zr}$  and  ${}^{209}_\Lambda\text{Pb}$ . The results have been obtained using some of the realistic Jülich and Nijmegen YN interactions; namely, the models Jülich B (JB) [75] and Jülich 04 (J04) [76], and the Nijmegen soft-core models NSC89 [77] and NSC97a-f [78, 79]. Results for the disoccupation of  $\Lambda$  bound and scattering states are also presented and discussed at the end of the section.

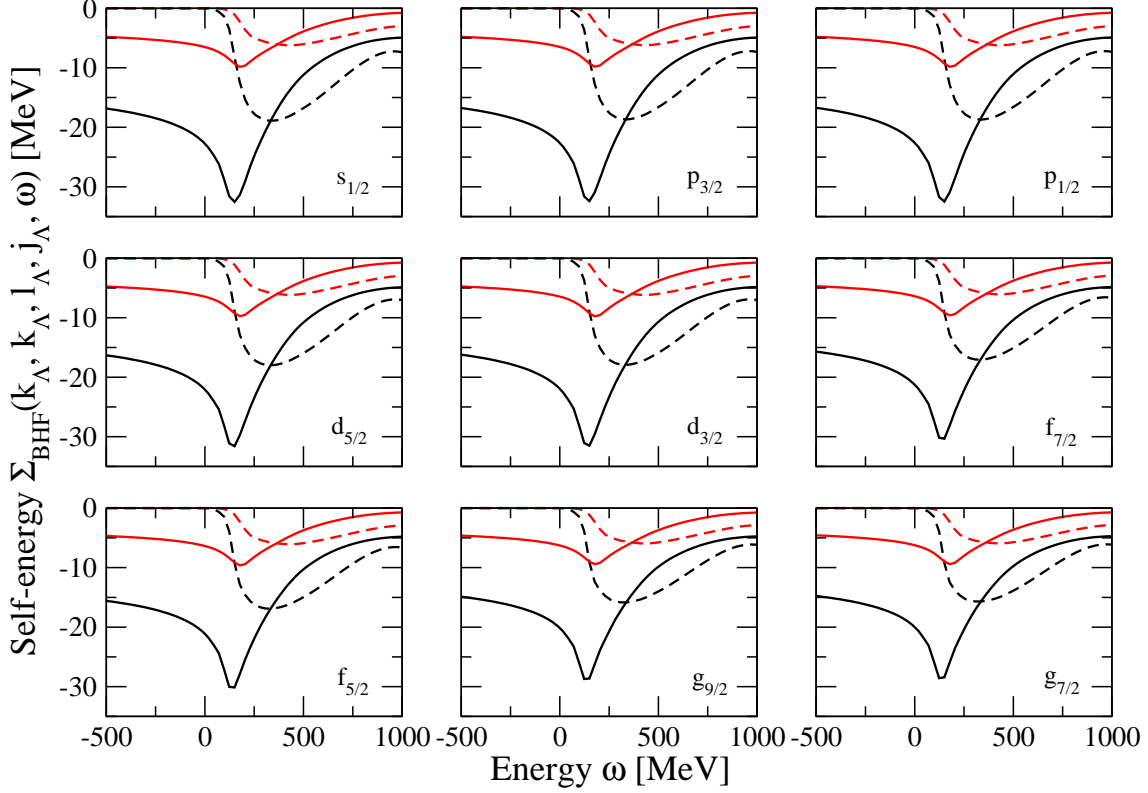


Figure 3: (color online) Energy dependence of the real  $\mathcal{V}$  (solid lines) and imaginary  $\mathcal{W}$  (dashed lines) part of the self-energy of a  $\Lambda$  with momenta of 300 (black lines) and 500 MeV/c (red lines) in the  $s, p, d, f$  and  $g$  partial waves for  $^{209}_{\Lambda}\text{Pb}$  obtained with the NSC89 model. The energy is measured with respect to the  $\Lambda$  rest mass.

### 3.1. $\Lambda$ self-energy

We start by showing in Fig. 2 the energy dependence of the real  $\mathcal{V}$  and imaginary  $\mathcal{W}$  part (see Eqs. (21) and (22)) of the self-energy of a  $\Lambda$  with momentum 300 MeV/c,  $l_{\Lambda} = 0$  and  $j_{\Lambda} = 1/2$ , for the six hypernuclei considered. Results are presented for all the YN interactions mentioned above. As it is seen in the figure, in general,  $\mathcal{W}$  is, in absolute value, larger in the Nijmegen models than in the Jülich ones. Consequently, the dispersion relation of Eq. (18) leads in the case of the Nijmegen models to a stronger energy dependence of  $\mathcal{V}$ . We observe that  $\mathcal{W}$  is only different from zero for  $\omega > 0$ , as it was said before, and that it is always negative, even for energies larger than those shown in the figure. Moreover, due to phase space restrictions,  $\mathcal{W}$  behaves almost quadratically for energies close to  $\omega = 0$  [84, 85]

$$\mathcal{W}(k_{\Lambda}, k'_{\Lambda}, l_{\Lambda}, j_{\Lambda}, \omega) \sim c\omega^2, \quad \omega \rightarrow 0^+. \quad (32)$$

The energy dependence of  $\mathcal{V}$  can be understood from the dispersion relation (18). Since  $\mathcal{W}$  is different from zero only for  $\omega > 0$  and it is negative, this dispersion relation implies that  $\mathcal{V}$  will be attractive for  $\omega < 0$ . This attraction increases up to a given positive value of  $\omega$  and then it

Nuclei	$l_{\Lambda}j_{\Lambda}$	JB	J04	NSC89	NSC97a	NSC97b	NSC97c	NSC97d	NSC97e	NSC97f	Exp.
${}^5_{\Lambda}\text{He}$	$s_{1/2}$	-2.28	-5.89	-0.58	-3.16	-3.38	-3.94	-4.24	-4.20	-3.59	$({}^5_{\Lambda}\text{He})$ -3.12
${}^{13}_{\Lambda}\text{C}$	$s_{1/2}$	-9.48	-18.94	-5.69	-11.46	-11.79	-12.76	-13.08	-12.82	-11.37	$({}^{13}_{\Lambda}\text{C})$ -11.69
	$p_{3/2}$		-3.66		-0.24	-0.32	-0.63	-0.68	-0.54	-0.01	-0.7 (p)
	$p_{1/2}$		-4.07		-0.12	-0.14	-0.37	-0.35	-0.19		
${}^{17}_{\Lambda}\text{O}$	$s_{1/2}$	-11.83	-23.40	-7.39	-14.31	-14.65	-15.70	-15.99	-15.68	-14.02	$({}^{16}_{\Lambda}\text{O})$ -12.5
	$p_{3/2}$	-0.87	-8.16		-2.57	-2.72	-3.24	-3.33	-3.10	-2.17	-2.5 (p)
	$p_{1/2}$	-1.06	-8.03		-2.16	-2.22	-2.61	-2.57	-2.30	-1.41	
${}^{41}_{\Lambda}\text{Ca}$	$s_{1/2}$	-19.60	-36.16	-15.04	-23.09	-23.42	-24.60	-24.74	-24.20	-21.96	$({}^{40}_{\Lambda}\text{Ca})$ -20.0
	$p_{3/2}$	-9.64	-23.81	-6.92	-12.37	-12.57	-13.40	-13.35	-12.84	-11.09	-12.0 (p)
	$p_{1/2}$	-9.92	-23.78	-6.29	-12.10	-12.23	-12.95	-12.78	-12.22	-10.45	
	$d_{5/2}$	-0.70	-11.72		-2.80	-2.93	-3.47	-3.38	-3.00	-1.83	-1.0 (d)
	$d_{3/2}$	-1.01	-11.65		-2.43	-2.46	-2.85	-2.61	-2.18	-1.04	
${}^{91}_{\Lambda}\text{Zr}$	$s_{1/2}$	-25.80	-46.30	-22.77	-31.38	-31.73	-33.05	-33.06	-32.33	-29.56	$({}^{89}_{\Lambda}\text{Y})$ -23.0
	$p_{3/2}$	-18.19	-37.73	-17.08	-23.92	-24.20	-25.28	-25.22	-24.58	-22.25	-16.0 (p)
	$p_{1/2}$	-18.30	-38.01	-16.68	-23.82	-24.06	-25.07	-24.92	-24.23	-21.88	
	$d_{5/2}$	-11.16	-28.35	-9.05	-14.41	-14.58	-15.36	-15.09	-14.42	-12.41	-9.0 (d)
	$d_{3/2}$	-11.17	-28.44	-8.49	-14.30	-14.40	-15.12	-14.77	-14.06	-11.99	
	$f_{7/2}$	-3.05	-18.45	-1.56	-5.46	-5.52	-6.03	-5.59	-4.93	-3.27	-2.0 (f)
	$f_{5/2}$	-2.99	-18.76	-1.00	-5.28	-5.26	-5.69	-5.20	-4.52	-2.86	
${}^{209}_{\Lambda}\text{Pb}$	$s_{1/2}$	-31.36	-59.95	-29.52	-38.85	-39.23	-40.63	-40.44	-39.50	-39.30	$({}^{208}_{\Lambda}\text{Pb})$ -27.0
	$p_{3/2}$	-27.13	-55.21	-26.01	-33.49	-33.91	-35.13	-34.80	-33.86	-31.03	-22.0 (p)
	$p_{1/2}$	-27.18	-55.40	-25.72	-33.38	-33.78	-34.94	-34.54	-33.56	-30.72	
	$d_{5/2}$	-21.70	-45.08	-17.85	-23.23	-23.54	-24.38	-23.79	-22.858	-20.60	-17.0 (d)
	$d_{3/2}$	-21.77	-45.07	-17.65	-23.17	-23.45	-24.27	-23.68	-22.75	-20.51	
	$f_{7/2}$	-13.00	-37.15	-9.67	-15.38	-15.43	-16.04	-15.05	-13.81	-10.98	-12.0 (f)
	$f_{5/2}$	-13.13	-37.16	-9.31	-15.35	-15.33	-15.90	-14.87	-13.61	-10.76	
	$g_{9/2}$	-8.14	-29.91	-5.27	-10.07	-10.14	-10.68	-9.80	-8.71	-6.28	-7.0 (g)
	$g_{7/2}$	-8.26	-30.16	-4.80	-10.01	-10.00	-10.46	-9.49	-8.37	-5.91	

Table 1: Energy of  $\Lambda$  single-particle bound states of several hypernuclei from  ${}^5_{\Lambda}\text{He}$  to  ${}^{209}_{\Lambda}\text{Pb}$  for the different YN interactions considered. Available experimental, data taken from Refs. [86, 87, 88], is shown for the closest measured hypernuclei. Units are given in MeV.

decreases, eventually turning into repulsion at large energies. Note that  $\mathcal{V}$  is more attractive for the heavier hypernuclei because their densities are larger.

All these features can be also observed in Fig. 3 where, for completeness, we show the energy dependence of  $\mathcal{V}$  and  $\mathcal{W}$  of a  $\Lambda$  in the  $s, p, d, f$  and  $g$  partial waves for  ${}^{209}_{\Lambda}\text{Pb}$ . The results are shown for the NSC89 model and two momenta of the hyperon: 300 and 500 MeV/c. Note that the dependence of both  $\mathcal{V}$  and  $\mathcal{W}$  on the orbital ( $l_{\Lambda}$ ) and total ( $j_{\Lambda}$ ) angular momentum of the  $\Lambda$  is rather weak. Note also that, as expected, the attraction of  $\mathcal{V}$  is clearly larger for the smaller momentum.

### 3.2. $\Lambda$ single-particle bound states

The energy of  $\Lambda$  single-particle bound states in  ${}^5_{\Lambda}\text{He}$ ,  ${}^{13}_{\Lambda}\text{C}$ ,  ${}^{17}_{\Lambda}\text{O}$ ,  ${}^{41}_{\Lambda}\text{Ca}$ ,  ${}^{91}_{\Lambda}\text{Zr}$  and  ${}^{209}_{\Lambda}\text{Pb}$  for the different YN interactions considered in this work are shown in Tab. 1. Note that we have considered only hypernuclei that are described as a closed shell nuclear core plus a  $\Lambda$  sitting in

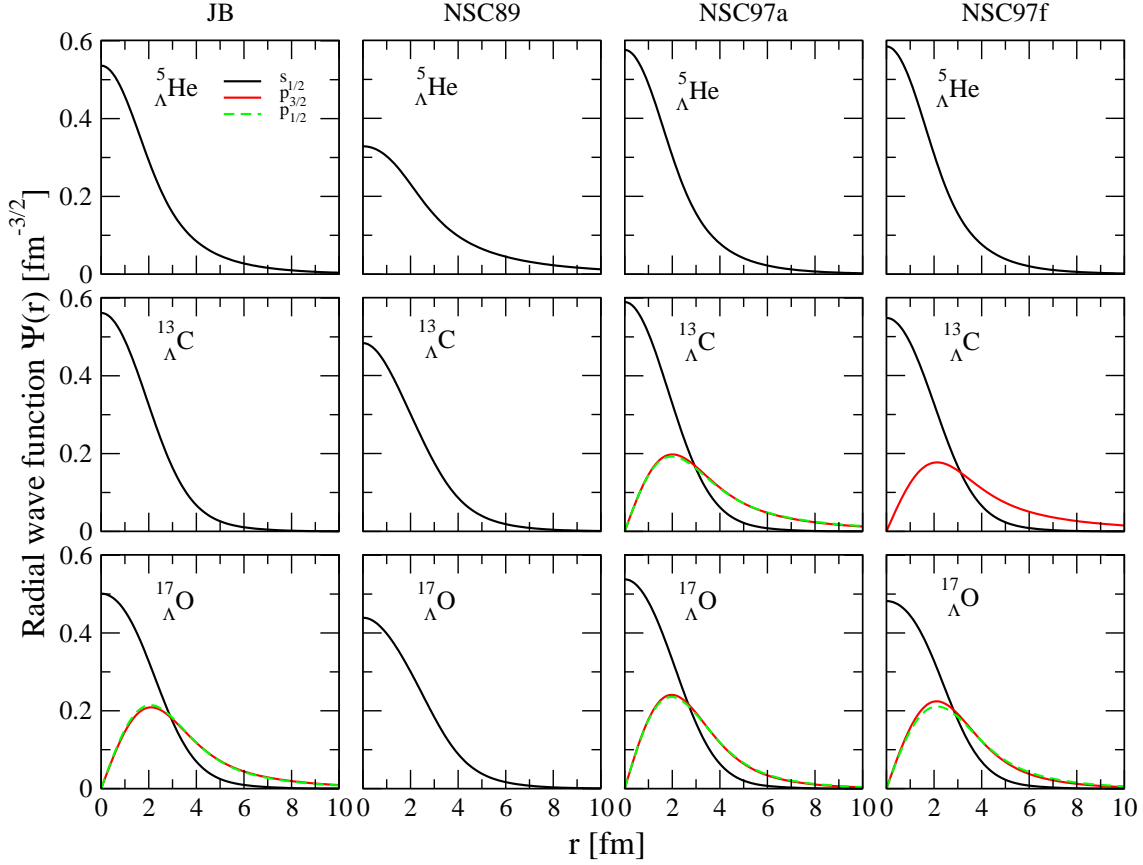


Figure 4: (color online) Radial wave function for the  $s$ - and  $p$ -wave states of a  $\Lambda$  hyperon in  ${}^5_{\Lambda}\text{He}$  (upper panels),  ${}^{13}_{\Lambda}\text{C}$  (middle panels) and  ${}^{17}_{\Lambda}\text{O}$  (lower panels) predicted by the JB, NSC89, NSC97a and NSC97f models.

a single-particle state. Since experimental data for those hypernuclei do not always exist, we show for comparison the closest representative hypernuclei for which experimental information is available. Experimental data have been taken from Refs. [86, 87, 88]. We note, however, that the differences between the calculated and the experimental values should not be associated only to this fact but mainly to the approximations used in the calculation or to the uncertainties of the interactions employed.

In general the agreement with experimental data is qualitatively good for most of the models except for the J04 one, which for all hypernuclei predicts an unrealistic overbinding of the  $\Lambda$  in all the single-particle states. For this reason, in the following we will not present further results for this model. Note that the results for  ${}^{91}_{\Lambda}\text{Zr}$  and  ${}^{209}_{\Lambda}\text{Pb}$  appear clearly overbound also for the other models, specially for the NSC97a-f ones. This overbinding is mainly due to two reasons. The first one is that the NSC97a-f models are too much attractive, predicting a  $\Lambda$  single-particle potential in symmetric nuclear matter of about  $-40$  MeV, in comparison with the value of around  $-30$  MeV extrapolated from hypernuclear data [89]. The second one is the fact that the distortion of the plane wave associated with the nucleon in the intermediate state of Fig. 1c, which is needed

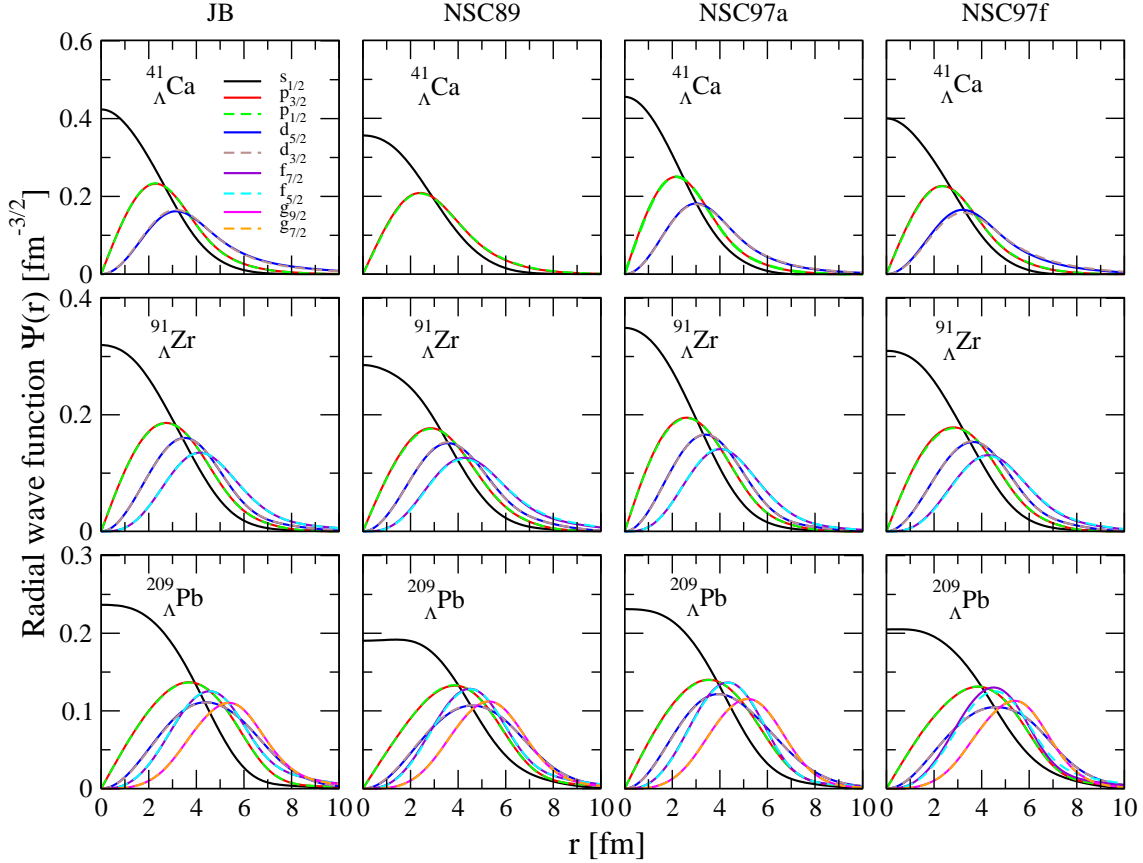


Figure 5: (color online) Radial wave function for the  $s$ -,  $p$ -,  $d$ -,  $f$ - and  $g$ -wave states of a  $\Lambda$  hyperon in  ${}^{41}_{\Lambda}\text{Ca}$  (upper panels),  ${}^{91}_{\Lambda}\text{Zr}$  (middle panels) and  ${}^{209}_{\Lambda}\text{Pb}$  (lower panels) predicted by the JB, NSC89, NSC97a and NSC97f models.

to guarantee its orthogonalization with the nucleon hole state (see *e.g.*, Ref. [80] for a detail description), has been done in an approximate way. In addition, the orthogonalization procedure has been optimized only for the case of  ${}^{17}_{\Lambda}\text{O}$ . Note finally that the splitting of the  $p$ -,  $d$ -,  $f$ - and  $g$ -wave states is of the order of few tenths of MeV in all cases due to the small spin-orbit strength of the YN interaction.

For completeness we plot in Figs. 4 and 5 the radial wave function of the  $\Lambda$  in the different bound states of the six hypernuclei considered. The results are shown only for the JB, NSC89, NSC97a and NSC97f YN interactions. Results for the NSC97b-e models are not shown because their difference with respect to those of the NSC97a and NSC97f is smaller than  $\sim 10\%$ . Therefore, from now on we will consider the NSC97a and NSC97f models together with the NSC89 one as representative of the Nijmegen Soft Core YN interaction.

The probability of finding the  $\Lambda$  at the center of the hypernucleus is given by  $|\Psi_{s_{1/2}}(r=0)|^2$ . As it can be seen in Figs. 4 and 5, going from light to heavy hypernuclei the wave function of the  $s_{1/2}$  state becomes more and more spread due to the larger extension of the nuclear density over which the  $\Lambda$  hyperon wants to be distributed and, therefore, this probability decreases. Only the

Nuclei	JB	NSC89	NSC97a	NSC97f
${}^5_{\Lambda}\text{He}$	3.08	4.83	2.79	2.70
${}^{13}_{\Lambda}\text{C}$	2.43	2.79	2.34	2.40
${}^{17}_{\Lambda}\text{O}$	2.47	2.80	2.39	2.47
${}^{41}_{\Lambda}\text{Ca}$	2.75	2.99	2.66	2.83
${}^{91}_{\Lambda}\text{Zr}$	3.15	3.31	3.01	3.20
${}^{209}_{\Lambda}\text{Pb}$	3.55	3.96	3.65	3.96

Table 2: Root-mean-square radius of the  $\Lambda$   $s_{1/2}$  bound state in several hypernuclei from  ${}^5_{\Lambda}\text{He}$  to  ${}^{209}_{\Lambda}\text{Pb}$  for the JB, NSC89, NSC97a and NSC97f models. Units are given in fm.

light hypernucleus  ${}^5_{\Lambda}\text{He}$  falls out of this pattern due to the fact that the energy of the bound state  $s_{1/2}$  is very small in this case, therefore, resulting in a very extended wave function, specially for the NSC89 model. Note now from Tab. 1 that, in fact, the NSC89 model predicts always the larger single-particle energies which result in the larger radii for all the bound  $\Lambda$  states and, therefore, in more extended wave functions than those predicted by the other models which are more localized. This is illustrated in particular for the  $s_{1/2}$  state in Tab. 2, where we show its root-mean-square radius for the different hypernuclei. Finally, we would like to conclude this discussion by noticing that, due to the scale of the figures, the small spin-orbit splitting of the  $p-$ ,  $d-$ ,  $f-$  and  $g-$  wave states cannot be resolved in the corresponding wave functions.

### 3.3. $\Lambda$ spectral function

In Fig. 6 we show the energy dependence of the continuum (solid lines) and discrete (dashed lines) contributions of the spectral function of a  $\Lambda$  with momentum 400 MeV/c,  $l_{\Lambda} = 0$  and  $j_{\Lambda} = 1/2$  for all the hypernuclei considered. The results have been obtained with the JB, NSC89, NSC97a and NSC97f YN interactions. The discrete contribution, as it was said at the end of Sec. 2, is a delta function with a strength given by Eq. (29), which is located at the energy of the single-particle  $s_{1/2}$  bound state of the corresponding hypernuclei (see Tab. 1). On the other hand, the strength of the continuum contribution is spread over all positive energies, and shows the well known quasi-particle peak at the value of the quasi-particle energy  $\varepsilon_{qp}^{l_{\Lambda}j_{\Lambda}}(k_{\Lambda})$ , which is defined through the following transcendental equation

$$\varepsilon_{qp}^{l_{\Lambda}j_{\Lambda}}(k_{\Lambda}) = \frac{\hbar^2 k_{\Lambda}^2}{2m_{\Lambda}} + \mathcal{V}(k_{\Lambda}, k_{\Lambda}, l_{\Lambda}, j_{\Lambda}, \varepsilon_{qp}^{l_{\Lambda}j_{\Lambda}}(k_{\Lambda})). \quad (33)$$

The quasi-particle peak is a reminiscence of the delta function structure of the spectral function of a non-interacting  $\Lambda$ . Note that this delta function should not be confused with that of the discrete contribution of the spectral function just described. The correlations between the  $\Lambda$  and the nucleons transform the simple delta function structure of the non-interacting case into the more complex one shown by the continuous lines of Fig. 6. They shift the position of the delta from its location at the kinetic energy of the  $\Lambda$  towards the value of  $\varepsilon_{qp}^{l_{\Lambda}j_{\Lambda}}(k_{\Lambda})$ , give it a width, and lower its strength which is distributed over all positive energies.

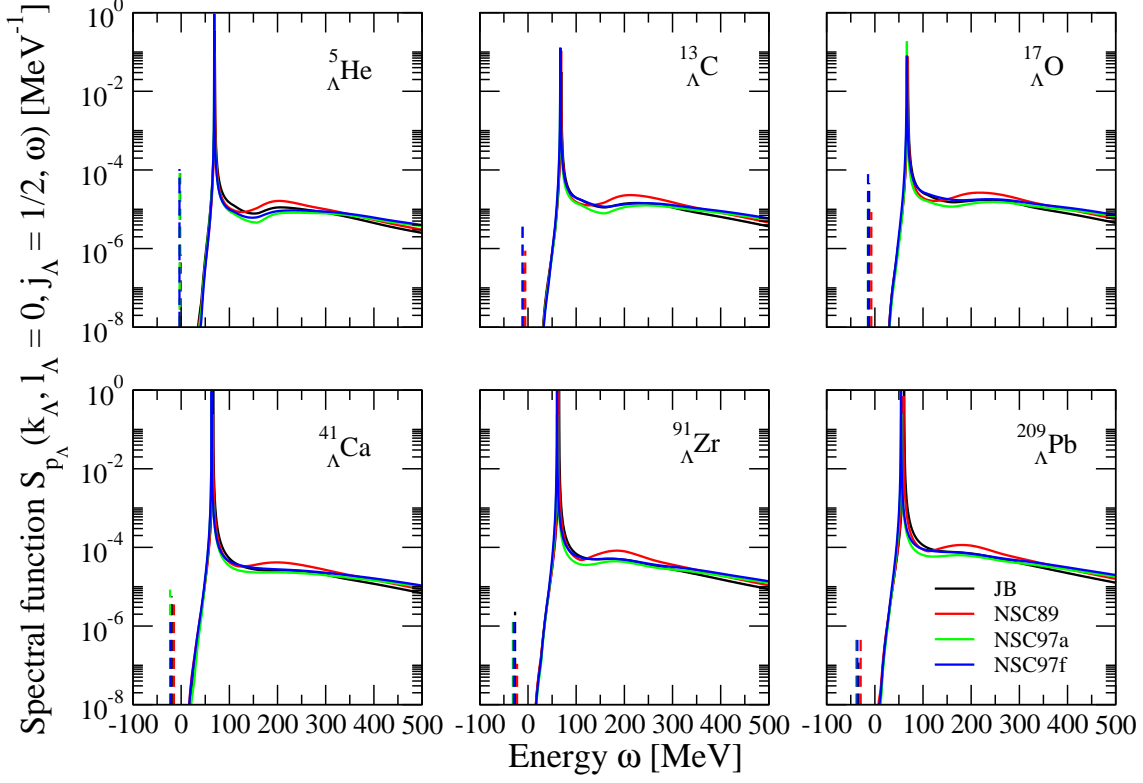


Figure 6: (color online) Energy dependence of the spectral function a  $\Lambda$  with momentum 400 MeV/c,  $l_\Lambda = 0$  and  $j_\Lambda = 1/2$  for several hypernuclei from  ${}^5_\Lambda\text{He}$  to  ${}^{209}_\Lambda\text{Pb}$  predicted by the JB (black lines), NSC89 (red lines), NSC97a (green lines) and NSC97f (blue lines) models. Solid and dashed lines show respectively the continuum and discrete contributions. The energy is measured with respect to the  $\Lambda$  rest mass.

An estimation of the role played by the  $\Lambda$ -nucleon correlations can be obtained from the measurement of the spectral strength that is located below the quasi-particle peak. This is given by the so-called  $\mathcal{Z}$ -factor, which is defined in a way similar to the spectroscopic one given in Eq. (30)

$$\mathcal{Z}_{l_\Lambda j_\Lambda}(k_\Lambda) = \left( 1 - \frac{\partial \mathcal{V}(k_\Lambda, k_\Lambda, l_\Lambda, j_\Lambda, \omega)}{\partial \omega} \Big|_{\omega=\varepsilon_{qp}^{l_\Lambda j_\Lambda}(k_\Lambda)} \right)^{-1}. \quad (34)$$

The smaller the value of  $\mathcal{Z}_{l_\Lambda j_\Lambda}(k_\Lambda)$  is, the more important are the correlations of the system. We show in Tab. 3 the value of  $\mathcal{Z}_{l_\Lambda j_\Lambda}(k_\Lambda)$  for three values of the momentum of a  $\Lambda$  with  $l_\Lambda = 0$  and  $j_\Lambda = 1/2$ . The corresponding value of  $\varepsilon_{qp}^{l_\Lambda j_\Lambda}(k_\Lambda)$  is also given. The results are shown, as before, for the JB, NSC89, NSC97a and NSC97f models. As it is seen, the value of  $\mathcal{Z}_{l_\Lambda j_\Lambda}(k_\Lambda)$  decreases when one moves from light to heavier hypernuclei. This simply reflects the fact that  $\Lambda$ -nucleon correlations becomes more and more important when the density of the nuclear core increases (see Fig. 2). The momentum dependence of  $\mathcal{Z}_{l_\Lambda j_\Lambda}(k_\Lambda)$  can be easily understand from the  $\Lambda$  self-energy. By looking at Fig. 3, it is clear that the energy dependence of the real part of the  $\Lambda$  self-energy is stronger for the smaller values of the momentum. Since the derivative of

Nuclei	$\hbar k_\Lambda$ (MeV/c)	JB	NSC89	NSC97a	NSC97f
${}^5_\Lambda\text{He}$	300	0.988 (36.58)	0.985 (36.64)	0.985 (34.62)	0.986 (34.36)
	400	0.993 (69.83)	0.991 (69.81)	0.992 (68.80)	0.992 (68.72)
	500	0.995 (111.04)	0.992 (110.97)	0.995 (110.45)	0.994 (110.44)
${}^{13}_\Lambda\text{C}$	300	0.980 (35.00)	0.974 (34.54)	0.976 (32.04)	0.975 (31.82)
	400	0.991 (68.95)	0.987 (68.55)	0.989 (67.26)	0.988 (67.21)
	500	0.994 (110.34)	0.990 (109.99)	0.993 (109.24)	0.992 (109.20)
${}^{17}_\Lambda\text{O}$	300	0.976 (34.31)	0.970 (33.74)	0.972 (30.97)	0.970 (30.69)
	400	0.989 (68.44)	0.986 (67.96)	0.988 (66.46)	0.986 (66.35)
	500	0.993 (109.98)	0.989 (109.57)	0.992 (108.67)	0.990 (108.59)
${}^{41}_\Lambda\text{Ca}$	300	0.965 (29.97)	0.956 (29.01)	0.961 (24.34)	0.957 (23.80)
	400	0.981 (66.52)	0.972 (65.82)	0.977 (63.46)	0.974 (63.28)
	500	0.989 (109.00)	0.982 (108.40)	0.987 (107.12)	0.985 (107.04)
${}^{91}_\Lambda\text{Zr}$	300	0.943 (26.68)	0.923 (24.95)	0.935 (19.31)	0.932 (18.70)
	400	0.978 (64.53)	0.966 (63.28)	0.976 (60.39)	0.971 (60.17)
	500	0.981 (107.80)	0.967 (106.82)	0.977 (105.18)	0.976 (105.05)
${}^{209}_\Lambda\text{Pb}$	300	0.913 (19.57)	0.902 (16.96)	0.918 (8.54)	0.913 (7.66)
	400	0.965 (60.83)	0.949 (58.95)	0.960 (54.63)	0.954 (54.31)
	500	0.974 (105.56)	0.952 (104.01)	0.967 (101.61)	0.966 (101.44)

Table 3:  $\mathcal{Z}$ -factor of a  $\Lambda$  with  $l_\Lambda = 0$  and  $j_\Lambda = 1/2$  and momenta 300, 400 and 500 MeV/c for several hypernuclei from  ${}^5_\Lambda\text{He}$  to  ${}^{209}_\Lambda\text{Pb}$  predicted by the JB, NSC89, NSC97a and NSC97f models. The value of the corresponding quasi-particle energy  $\varepsilon_{qp}^{l_\Lambda j_\Lambda}(k_\Lambda)$  is given in brackets in units of MeV.

$\mathcal{V}$  is negative at the quasi-particle energy, and larger in absolute value for the smaller momenta, the  $\mathcal{Z}$ -factor decreases when decreasing the momentum of the  $\Lambda$ , as it is seen in the table. We note, however, that the  $\mathcal{Z}$ -factor is, in general, relatively large. This is in agreement with the fact, already mentioned in the introduction, that the  $\Lambda$  keeps its identity inside the nucleus, and that is less correlated than the nucleons for which the  $\mathcal{Z}$ -factor is smaller. This was already observed in nuclear matter by Robertson and Dickhoff in Refs. [72, 73].

We finish this part of the section by showing in Fig. 7 a weighted sum of the  $\Lambda$  spectral function defined as

$$S(k_\Lambda, \omega) = \sum_{l_\Lambda j_\Lambda} (2j_\Lambda + 1) S_{p_\Lambda}(k_\Lambda, l_\Lambda, j_\Lambda, \omega). \quad (35)$$

The results have been obtained with the NSC97f model, and are given for all the hypernuclei and three momenta of the  $\Lambda$ . As in Fig. 6, solid and dashed lines show the continuum and discrete contributions. The figure presents the same general features described before and, therefore, there is no need to discuss them again. Note simply that the discrete contribution of  $S(k_\Lambda, \omega)$  is a set of weighted delta functions located at the energies of the corresponding bound states (see Tab. 1), and that the quasi-particle peak of the continuum, as it is well known, moves towards larger energies when the momentum of the  $\Lambda$  increases (see also the last column of Tab. 3).

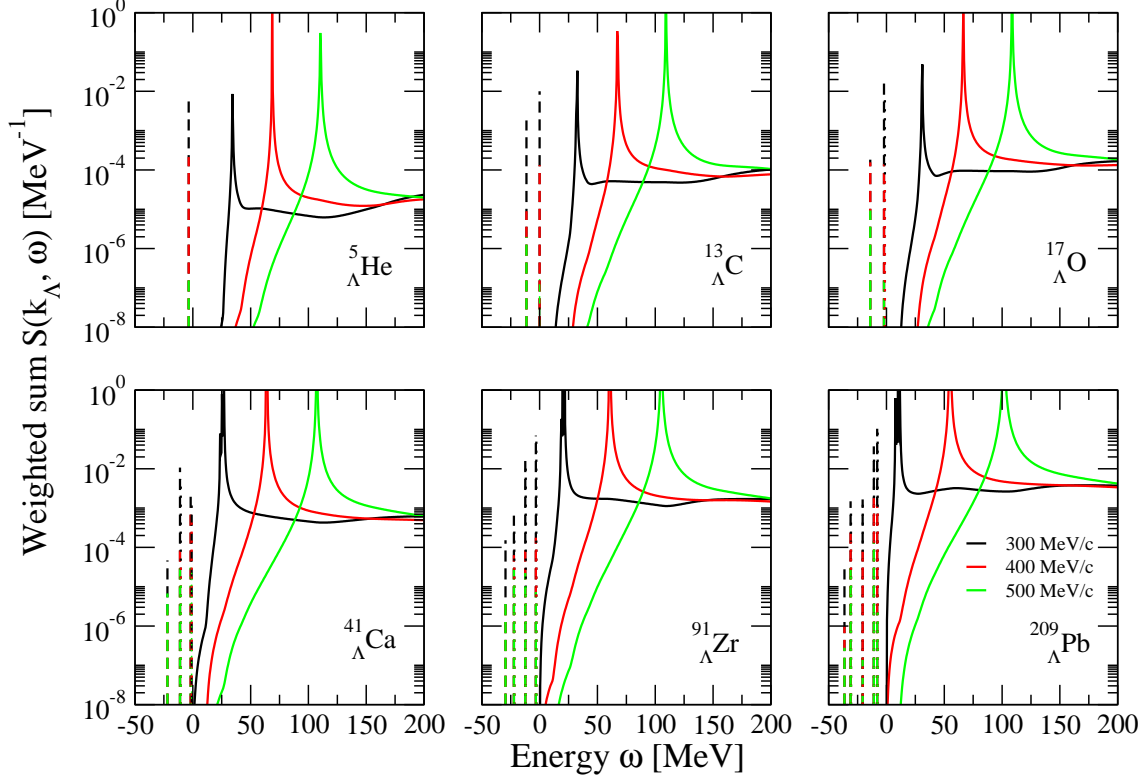


Figure 7: (color online) Energy dependence of the weighted sum of the spectral function (see Eq. (35)) of a  $\Lambda$  with momentum 300 (black lines), 400 (red lines) and 500 (green lines) MeV/c for several hypernuclei from  ${}^5_{\Lambda}\text{He}$  to  ${}^{209}_{\Lambda}\text{Pb}$  predicted by the NSC97f model. Solid and dashed lines show respectively the continuum and discrete contributions. The energy is measured with respect to the  $\Lambda$  rest mass.

### 3.4. Disoccupation number

To finish this section, we show in Figs. 8 and 9, respectively, the disoccupation of the  $s_{1/2}$  state in the different hypernuclei, and that of the  $s-$ ,  $p-$ ,  $d-$ ,  $f-$  and  $g-$  wave ones in  ${}^{209}_{\Lambda}\text{Pb}$ , predicted by the JB and the NSC97f models. In both figures, the discrete (solid lines) and continuum (dashed lines) contributions are shown separately. It is clear from Eqs. (12) and (23) that the sum of both contributions is 1. In general, as it has been already said, a  $\Lambda$  with quantum numbers  $k_{\Lambda}l_{\Lambda}j_{\Lambda}$  can be always be added to the nucleus, either in a bound state with probability

$$d^d(k_{\Lambda}, l_{\Lambda}, j_{\Lambda}) = \int_{\mu_{\Lambda}}^{\infty} d\omega S_{p_{\Lambda}}^d(k_{\Lambda}, l_{\Lambda}, j_{\Lambda}, \omega), \quad (36)$$

or in a scattering one with probability

$$d^c(k_{\Lambda}, l_{\Lambda}, j_{\Lambda}) = \int_{\mu_{\Lambda}}^{\infty} d\omega S_{p_{\Lambda}}^c(k_{\Lambda}, l_{\Lambda}, j_{\Lambda}, \omega) = 1 - d^d(k_{\Lambda}, l_{\Lambda}, j_{\Lambda}). \quad (37)$$

Intuitively, one expects that if the momentum  $k_{\Lambda}$  is large, then the  $\Lambda$  can easily escape and, therefore, the probability of binding it in the nucleus should be quite small. This feature is

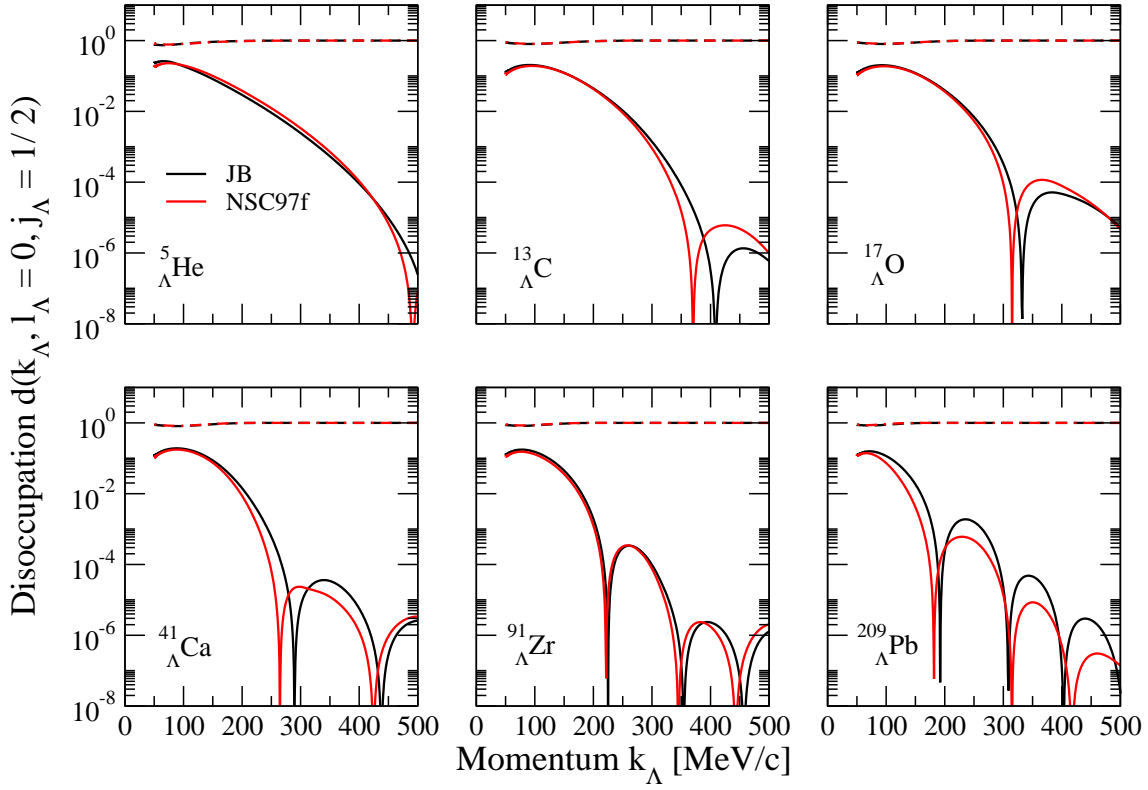


Figure 8: (color online) Disoccupation of the  $s_{1/2}$  state in different hypernuclei from  ${}^5_{\Lambda}\text{He}$  to  ${}^{209}_{\Lambda}\text{Pb}$  obtained with the JB (black lines) and NSC97f (red lines) models. Solid and dashed lines show respectively the discrete and continuum contributions.

clearly shown in both figures, where we can observe that, in fact, the discrete contribution to the disoccupation of a given  $l_{\Lambda}j_{\Lambda}$  state is always much smaller than the continuum one being, in fact, almost negligible for large values of the momentum of the  $\Lambda$ . This indicates that in hypernuclear production reactions the  $\Lambda$  hyperon is formed mostly in a quasi-free state. We note finally that the oscillation behaviour of  $d^d(k_{\Lambda}, l_{\Lambda}, j_{\Lambda})$  is simply due to the zeros of the projection coefficient  $\langle k_{\Lambda}l_{\Lambda}j_{\Lambda}|\Psi\rangle$  (see Eq. (29)), that in the logarithmic scale of the plot appear as singularities.

#### 4. Summary and conclusions

In this work we have determined the single-particle spectral function of the  $\Lambda$  hyperon in several hypernuclei. To such end, we have obtained first the corresponding  $\Lambda$  self-energy using a perturbative many-body approach with some of the realistic YN interactions of the Jülich [75, 76] and the Nijmegen [77, 78, 79] groups. The calculation started with the construction of a nuclear matter YN  $G$ -matrix that was used to build a finite nuclei one through a perturbative expansion that is truncated at second order. This finite nuclei YN  $G$ -matrix was then employed to calculate the  $\Lambda$  self-energy. From it we obtained finally the  $\Lambda$  spectral function and the binding energies, wave functions and disoccupation numbers of different single-particle states for various

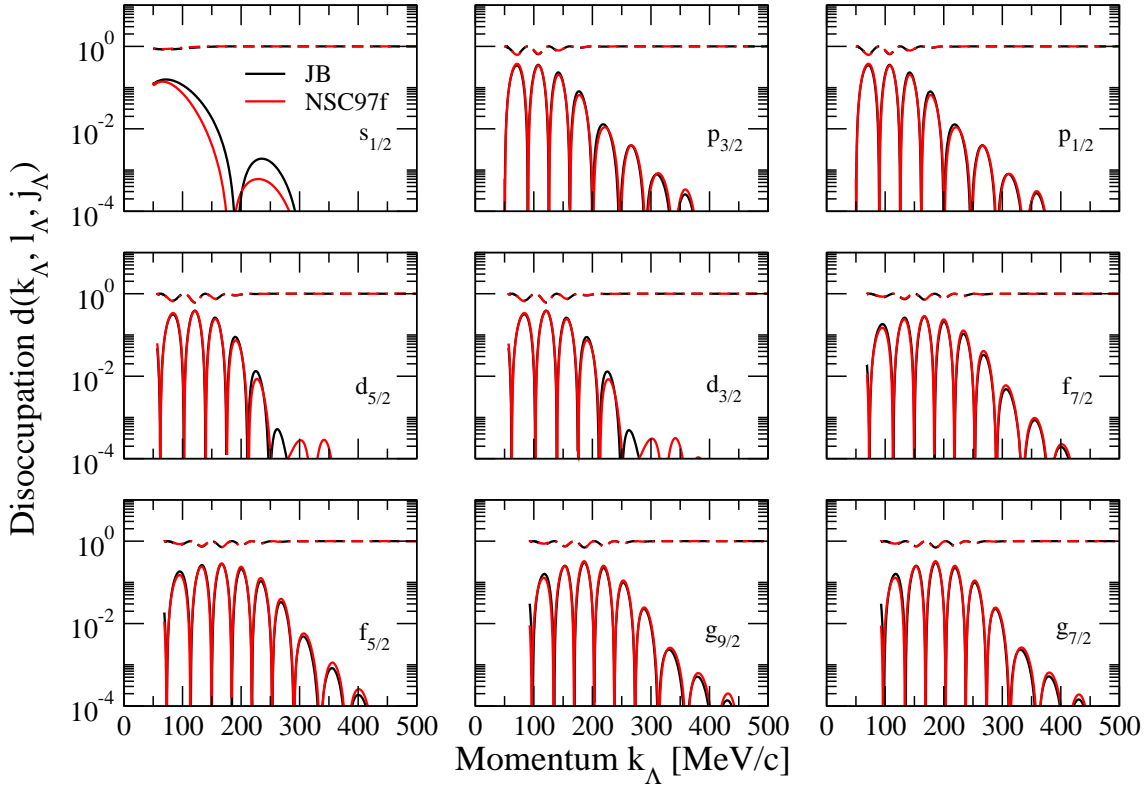


Figure 9: (color online) Disoccupation of the  $s$ -,  $p$ -,  $d$ -,  $f$ - and  $g$ -wave states in  $^{209}_{\Lambda}\text{Pb}$  obtained with the JB (black lines) and NSC97f (red lines) models. Solid and dashed lines show respectively the discrete and continuum contributions.

hypernuclei from  $^5_{\Lambda}\text{He}$  to  $^{209}_{\Lambda}\text{Pb}$ .

We showed that the Nijmegen models predict an imaginary part of the  $\Lambda$  self-energy larger than that obtained with the Jülich ones, which results in a stronger energy dependence of its real part. The dependence of the  $\Lambda$  self-energy on the orbital ( $l_{\Lambda}$ ) and total ( $j_{\Lambda}$ ) angular momentum of the  $\Lambda$  was found to be quite small.

Using the real part of the  $\Lambda$  self-energy as an effective hyperon-nucleus potential in the Schrödinger equation, we obtained the  $\Lambda$  single-particle bound states in the several hypernuclei considered. Our results compared rather well with the experimental data for all the models except for the J04, which predicted an unrealistic overbinding of all the  $\Lambda$  single-particle orbits. The small spin-orbit splitting of the  $p$ -,  $d$ -,  $f$ - and  $g$ -wave states was confirmed.

The discrete and the continuum contributions of the single- $\Lambda$  spectral function were then obtained from the  $\Lambda$  self-energy. Their appearance was found to be qualitatively similar to that of the nucleons. We showed that the discrete contribution is a weighed delta function located at the energy of the corresponding single- $\Lambda$  bound state, and that the strength of the continuum one is spread over all positive energies showing the well known quasi-particle peak at the corresponding energy. The so-called  $\mathcal{Z}$  factor, that measures the importance of the correlations, was also calculated for the  $s_{1/2}$  state. Our results showed that the value of  $\mathcal{Z}$  was relatively large, indi-

cating that the  $\Lambda$  is less correlated than the nucleons, in agreement with the idea that it maintains its identity inside the nucleus, and with the results of a previous study of the  $\Lambda$  correlations in infinite nuclear matter [72, 73].

Finally, by integrating the  $\Lambda$  spectral function over the energy, we obtained the disoccupation numbers of different single-particle states for the various hypernuclei. Our results showed that the discrete contribution to the disoccupation numbers is always much more smaller than the continuum one, indicating that in hypernuclear production reactions the  $\Lambda$  hyperon is formed mostly in a quasi-free state. To finish, we would like to say that scattering reactions, such as the high precision ( $e, e'K^+$ ) ones carried out at JLAB and MAMI-C, can provide valuable information on the disoccupation of  $\Lambda$  single-particle bound states needed to have a more complete description of the properties of the  $\Lambda$  hyperon in nuclear systems.

## Acknowledgements

The author wants to express his deep gratitude to Artur Polls for all the useful and stimulating conversations they had during the development of this work. This work is supported by the NewCompstar, COST Action MP1304.

## References

### References

- [1] M. Danysz and J. Pniewski, *Phil. Mag.* **44**, 348 (1953).
- [2] M. Juric *et al.*, *Nucl. Phys. B* **52**, 1 (1973).
- [3] D. H. Davis in *Proceedings of the LAMP Workshop on ( $\pi, K$ ) Physics*, AIP Conf. Proc. **224**, edited by B. F. Gibson, W. R. Gibbs and M. B. Johnson, p. 38 (AIP, New York 1991).
- [4] M. Danysz *et al.*, *Phys. Rev. Lett.* **11**, 29 (1963).
- [5] M. Danysz *et al.*, *Nucl. Phys. A* **49**, 121 (1963).
- [6] R. H. Dalitz, D. H. Davis, P. H. Fowler, A. Montwill, J. Pniewski and J. A. Zakrewski, *Proc. Roy. Soc. London, Ser. A* **426**, 1 (1989).
- [7] D. J. Prowse, *Phys. Rev. Lett.* **17**, 782 (1966).
- [8] S. Aoki *et al.*, *Prog. Theor. Phys.* **85**, 1287 (1991).
- [9] C. B. Dover, D. J. Millener, A. Gal and D. H. Davis, *Phys. Rev. C* **44**, 1905 (1991).
- [10] G. B. Franklin, *Nucl. Phys. A* **585**, 83c (1995).
- [11] E. V. Hugenford, *Prog. Theor. Phys. Suppl.* **117**, 135 (1994).
- [12] S. Bianchin *et al.*, *Int. J. Mod. Phys. E* **18**, 2187 (2009).

- [13] C. Rappold *et al.*, Nucl. Phys. A **913**, 170 (2013).
- [14] H. Takahashi *et al.*, Phys. Rev. Lett. **87**, 212502 (2001).
- [15] P. Kaustov *et al.*, Phys. Rev. C **61**, 054603 (2000).
- [16] K. Nakazawa *et al.*, Prog. Theor. Exp. Phys. (2015) 0033D02.
- [17] A. Bouyssy and J. Hüfner, Phys. Lett. B **64**, 276 (1976).
- [18] A. Bouyssy, Phys. Lett. B **84**, 42 (1979).
- [19] C. D. Dover, L. Ludeking and G. E. Walker, Phys. Rev. C **22**, 2073 (1980).
- [20] T. Motoba, H. Bandō, T. Fukuda and J. Žofka Phys. Rev. C **38**, 1322 (1988).
- [21] D. J. Millener, C. B. Dover and A. Gal, Phys. Rev. C **38**, (1988) 2700.
- [22] Y. Yamamoto, H. Bandō and J. Žofka, Prog. Theor. Phys. **80**, (1988) 757.
- [23] F. Fernández, T. López-Arias and C. Prieto, Z. Phys. A **334**, (1989) 349.
- [24] D. E. Lansky and Y. Yamamoto, Phys. Rev. C **55**, 2330 (1997).
- [25] T. Y. Tretyakova and D. E. Lankoy, Eur. Phys. J. A **5**, 391 (1999).
- [26] J. Cugnon, A. Lejeune, and H.-J. Schulze, Phys. Rev. C **62**, 064308 (2000).
- [27] I. Vidaña, A. Polls, A. Ramos and H.-J. Schulze, Phys. Rev. C **64**, 044301 (2001).
- [28] X. -R. Zhou, H.-J. Schulze, H. Sagawa, C.-X. Wu and E.-G. Zhao, Phys. Rev. C **76**, 034312 (2007).
- [29] X.-R. Zhou, A. Polls, H.-J. Schulze and I. Vidaña, Phys. Rev. C **78**, 054306 (2008).
- [30] J. Mareš and J. Žofka, Z. Phys. A **33**, 209 (1989).
- [31] N. K. Glendenning, D. Von-Eiff, M. Haft, H. Lenske and M. K. Weigel, Phys. Rev. C **48**, 889 (1993).
- [32] J. Mareš and B. K. Jennings, Phys. Rev. C **49**, 2472 (1994).
- [33] Y. Sugahara and H. Toki, Prog. Theor. Phys. **92**, 803 (1994).
- [34] R. J. Lombard, S. Marcos and J. Mareš, Phys. Rev. C **51**, 1784 (1995).
- [35] Z. Ma, J. Speth, S. Krewald, B. Chen and A. Reuber, Nucl. Phys. A **608**, 305 (1996).
- [36] F. Ineichenm, D. Von-Eiff and M. K. Weigel, J. Phys. G **22**, 1421 (1996).
- [37] K. Tsushima, K. Saito and A. W. Thomas, Phys. Lett. B **411**, 9 (1997).

- [38] K. Tsushima, K. Saito, J. Haidenbauer and A. W. Thomas, Nucl. Phys. A **630**, 691 (1998).
- [39] E. N. E. van Dalen, G. Colucci and A. Sedrakian, Phys. Lett. B **734**, 383 (2014).
- [40] R. Brockmann and W. Weise, Nucl. Phys. A **355**, 365 (1981).
- [41] M. Chiapparini, A. O. Gattone and B. K. Jennings, Nucl. Phys. A **529**, 589 (1991).
- [42] Y. Yamamoto and H. Bandō, Prog. Theor. Phys. Suppl. **81**, 9 (1985).
- [43] Y. Yamamoto and H. Bandō, Prog. Theor. Phys. **83**, 254 (1990).
- [44] Y. Yamamoto, A. Reuber, H. Himeno, S. Nagata and T. Motoba, Cze. Jour. Phys. **42**, 1249 (1992).
- [45] Y. Yamamoto, A. Reuber, H. Himeno, S. Nagata and T. Motoba, Prog. Theor. Phys. Suppl. **117**, 361 (1994).
- [46] D. Halderson, Phys. Rev. C **48**, 581 (1993).
- [47] J. Hao, T. T. S. Kuo, A. Reuber, K. Holinde, J. Speth and D. J. Millener, Phys. Rev. Lett. **71**, 1498 (1993).
- [48] M. Hjorth–Jensen, A. Polls, A. Ramos and H. Mütter, Nucl. Phys. A **605**, 458 (1996).
- [49] I. Vidaña, A. Polls, A. Ramos and M. Hjorth–Jensen, Nucl. Phys. A **644**, 201 (1998).
- [50] I. Vidaña, *Description of hyperonic matter and hypernuclei within the Brueckner–Hartree–Fock theory*, Ph.D. Thesis, University of Barcelona (2001). <http://www.tesisenxarxa.net/handle/10803/1583>
- [51] D. Lonardoni, S. Gandolfi and F. Pederiva, Phys. Rev. C **87**, 041303 (R) (2013).
- [52] D. Lonardoni, F. Pederiva and S. Gandolfi, Phys. Rev. C **89**, 014314 (2014).
- [53] O. Benhar, A. Fabrocini and S. Fantoni, Nucl. Phys. A **505**, 267 (1989).
- [54] O. Benhar, A. Fabrocini and S. Fantoni, Phys. Rev. C **41**, R24 (1990).
- [55] O. Benhar, A. Fabrocini and S. Fantoni, Nucl. Phys. A **550**, 201 (1992).
- [56] W. H. Dickhoff and H. Mütter, Rep. Prog. Phys. **55**, 1947 (1992).
- [57] O. Benhar, V. R. Pandharipande and S. C. Pieper, Rev. Mod. Phys. **65**, 817 (1993).
- [58] H. Mütter and W. H. Dickhoff, Phys. Rev. C **49**, R17, (1994).
- [59] D. Van Neck, A. E. L. Dieperink and E. Moya de Guerra, Phys. Rev. C **51**, 1800 (1994).
- [60] H. Mütter, A. Polls and W. H. Dickhoff, Phys. Rev. C **51**, 3040 (1995).

- [61] C. Ciofi degli Atti and S. Simula, Phys. Rev. C **53**, 1689 (1995).
- [62] W. J. W. Geurts, K. Allaart, W. H. Dickhoff and H. Mütter, Phys. Rev. C **54**, 1144 (1996).
- [63] H. Mütter and A. Polls, Prog. Part. Nucl. Phys. **45**, 243 (2000).
- [64] W. H. Dickhoff and C. Barbieri, Prog. Part. Nucl. Phys. **52**, 377 (2004).
- [65] T. Frick, H. Mütter and A. Polls, Phys. Rev. C **69**, 054305 (2004).
- [66] T. Frick, H. Mütter, A. Rios, A. Polls and A. Ramos, Phys. Rev. C **71**, 014313 (2005).
- [67] O. Benhar, D. Day and I. Sick, Rev. Mod. Phys. **80**, 189 (2008).
- [68] A. Rios, A. Polls and I. Vidaña, Phys. Rev. C **79**, 025802 (2009).
- [69] A. Rios, A. Polls and W. H. Dickhoff, Phys. Rev. C **79**, 064308 (2009).
- [70] H. Dussan, S. J. Waldecker, W. H. Dickhoff, H. Mütter and A. Polls, Phys. Rev. C **84**, 044319 (2011).
- [71] A. Carbone, A. Cipollone, C. Barbieri, A. Rios and A. Polls, Phys. Rev. C **88**, 054326 (2013).
- [72] N. J. Robertson, *Effects of short-range correlations on  $\Lambda$  decay in nuclear matter*, Ph.D. Thesis, Washington University (2003).
- [73] N. J. Robertson and W. H. Dickhoff, Phys. Rev. C **70**, 044301 (2004).
- [74] A. L. Fetter and J. D. Walecka, *Quantum Theory of Many-Particle Systems*, McGraw-Hill Book Company, New-York 1971.
- [75] B. Holzenkamp, K. Holinde and J. Speth, Nucl. Phys. A **500**, (1989) 485.
- [76] J. Haidenbauer and U.-G. Meissner, Phys. Rev. C **72**, (2005) 044005.
- [77] P. M. M. Maesen, T. A. Rijken and J. J. de Swart, Phys. Rev. C **40**, (1989) 2226.
- [78] T. A. Rijken, V. G. J. Stoks and Y. Yamamoto, Phys. Rev. C **59**, (1999) 21.
- [79] V. G. J. Stoks and T. A. Rijken, Phys. Rev. C **59**, (1999) 3009.
- [80] M. Borromeo, D. Bonatsos, H. Mütter and A. Polls, Nucl. Phys. A **539**, 189 (1992).
- [81] M. Hjorth-Jensen, H. Mütter and A. Polls, Phys. Rev. C **50**, 501 (1994).
- [82] J. Hao, T. S. S. Kuo, A. Reuber, K. Holinde, J. Speth and D. J. Millener, Phys. Rev. Lett. **71**, 1498 (1993).
- [83] D. Halderson, Phys. Rev. C **48**, 581 (1993).

- [84] J. M. Luttinger, Phys. Rev. **121**, 942 (1961).
- [85] R. Sartor, Phys. Lett. B **69**, 6 (1977).
- [86] H. Bandō, T. Motova and J. Žofka, Int. J. Mod. Phys. A **5**, 4021 (1990).
- [87] P. H. Pile *et al.*, Phys. Rev. Lett. **66**, 2585 (1991).
- [88] T. Hasegawa *et al.*, Phys. Rev. C **53**, 1210 (1996).
- [89] D. J. Millener, C. B. Dover and A. Gal, Phys. Rev. C **38**, 2700 (1988).